Global simulation of tropospheric ozone using the University of Maryland Chemical Transport Model (UMD-CTM): 2. Regional transport and chemistry over the central United States using a stretched grid

R. J. Park,[1] K. E. Pickering, and D. J. Allen
Department of Meteorology, University of Maryland, College Park, Maryland, USA

G. L. Stenchikov
Department of Environmental Sciences, Rutgers University, New Brunswick, New Jersey, USA

M. S. Fox-Rabinovitz
Earth System Science Interdisciplinary Center, University of Maryland, College Park, Maryland, USA

Received 21 October 2003; revised 24 February 2004; accepted 5 March 2004; published 8 May 2004.

[1] We use the stretched-grid version of the three-dimensional global University of Maryland Chemical Transport Model (UMD-CTM) to examine the effects of mesoscale meteorological features such as fronts and deep convection on regional-scale chemistry and transport. The stretched-grid model simulation, with a grid configuration featuring a mesoscale resolution region centered over the central United States, was conducted for June 1985, and evaluated through comparisons with a set of aircraft observations of trace gases. We also present results from a uniform-grid UMD-CTM simulation with a more conventional $2° \times 2.5°$ horizontal resolution for the same time period to examine how well the stretched-grid global model simulates mesoscale features. The changes in middle and upper tropospheric CO and O_3 due to convection from the model simulations are in good agreement with the range of measurements. The stretched-grid model shows better agreement with measurements than the uniform-grid model for the enhancement of trace gases in upper troposphere outflow due to deep convection and for the gradient of trace gas mixing ratios across a cold front. Peak convective enhancement of CO in the upper troposphere is larger in the stretched-grid model simulation than in the uniform-grid simulation, indicating a better representation of locally focused deep convective transport of polluted boundary layer air in the former. This type of vertical transport feature must be handled accurately if a model is to be used for intercontinental transport calculations. However, we find that deep convection in both model simulations, although better simulated in the stretched-grid model, is too widespread and too frequent. We find that net ozone production in the polluted boundary layer is ~15% less in the fine-grid region (0.5° resolution) of the stretched-grid model than in the same region of the $2° \times 2.5°$ model due to less artificial dilution of ozone precursors. The net ozone production in convective outflow plumes is also smaller in the stretched-grid model than in the uniform-grid model. We estimate the net flux of ozone from North America in the lowest 7 km to be 10 Gmol d^{-1} for the month of June using the results from the stretched-grid simulation. This value includes direct horizontal boundary layer flux, ozone that has been vertically transported from the boundary layer to free troposphere, and ozone that had been produced photochemically in the free troposphere. *INDEX TERMS:* 0345 Atmospheric Composition and Structure: Pollution—urban and regional (0305); 0368 Atmospheric Composition and Structure: Troposphere—constituent transport and chemistry; 3314 Meteorology and Atmospheric Dynamics: Convective processes; 3324 Meteorology and Atmospheric Dynamics: Lightning;

[1]Now at Division of Engineering and Applied Sciences, Department of Earth and Planetary Sciences, Harvard University, Cambridge, Massachusetts, USA.

0148-0227/04/2003JD004269$09.00

3329 Meteorology and Atmospheric Dynamics: Mesoscale meteorology; *KEYWORDS:* ozone, regional downscaling, pollution export

Citation: Park, R. J., K. E. Pickering, D. J. Allen, G. L. Stenchikov, and M. S. Fox-Rabinovitz (2004), Global simulation of tropospheric ozone using the University of Maryland Chemical Transport Model (UMD-CTM): 2. Regional transport and chemistry over the central United States using a stretched grid, *J. Geophys. Res.*, *109*, D09303, doi:10.1029/2003JD004269.

1. Introduction

[2] In recent years intercontinental transport of air pollutants has been noted in observations and in model simulations. For example, Asian emissions have been detected entering the west coast of the United States [*Jaffe et al.*, 1999]. Global chemical transport models (CTMs) also show impacts of Asian pollution on North American air quality [e.g., *Berntsen et al.*, 1999; *Jacob et al.*, 1999]. North American emissions affect trace gas mixing ratios over the North Atlantic and in parts of Europe [e.g., *Li et al.*, 2002]. Deep convection is one of the mechanisms through which pollutants are vented from the boundary layer and rapidly exported from source regions. *Crutzen and Gidel* [1983], *Gidel* [1983], and *Chatfield and Crutzen* [1984] hypothesized that convective clouds play an important role in rapid atmospheric vertical transport of trace species on a global basis and tested parameterizations of convective transport in chemical transport models. *Dickerson et al.* [1987] documented strong evidence of deep convective transport through in situ observations. Several subsequent flight projects [e.g., *Pickering et al.*, 1996; *Hauf et al.*, 1995; *Folkins et al.*, 1997; *Jonquières and Marenco*, 1998] have shown nearly undiluted boundary layer air containing reactive tracers in thunderstorm anvils reaching the tropopause level. Because of the stronger winds and the much longer chemical lifetimes of species in the middle and upper troposphere, convective transport plays a significant role in determining the chemical composition of the atmosphere and the magnitude of intercontinental transport.

[3] Several researchers have examined the effect of deep convective clouds on tropospheric chemistry using two-dimensional (2-D) and three-dimensional (3-D) cloud-resolving models [e.g., *Pickering et al.*, 1992a, 1992b; *Wang et al.*, 1995; *Hauf et al.*, 1995; *Pickering et al.*, 1996; *Wang and Prinn*, 2000; *Lu et al.*, 2000; *DeCaria et al.*, 2000; *Barth et al.*, 2001]. These models generally include detailed cloud microphysics and are nonhydrostatic. However, they are quite limited in terms of time and space due to the extensive computations that are necessary. They have been used for detailed studies of the effects of individual convective events on tropospheric chemistry. Alternatively, one-dimensional CTMs with parameterized convection have been used [*Wang et al.*, 2000; *Park et al.*, 2001].

[4] *Lelieveld and Crutzen* [1994] demonstrated the importance of convective transport for the global distribution of ozone using a global 3-D CTM, and *Lawrence et al.* [2003] have further clarified this role. Deep convection has been incorporated in most global 3-D CTMs [e.g., *Müller and Brasseur*, 1995; *Roelofs and Lelieveld*, 1995; *Brasseur et al.*, 1996; *Wang et al.*, 1998; *Brasseur et al.*, 1998; *Bey et al.*, 2001; *Park et al.*, 2004] used for tropospheric chemistry research. Such models typically operate on grids with no finer than 2-degree horizontal resolution. However, typical deep convective clouds are on the order of tens of kilometers in size, and, hence, must be treated as a sub-grid scale process in current global models. Therefore global 3-D CTMs employ various parameterizations to address convective processes. However, these parameterizations are insufficiently verified on a global scale.

[5] Global chemical transport models are required for calculating intercontinental transport. For accurate estimation of pollutant export from a continent, urban plumes need to be simulated in sufficient detail such that ozone production is reasonably represented. Ozone is one of the gases with a sufficiently long lifetime in the free troposphere such that it may be transported from one continent to another. Urban plume representation requires mesoscale horizontal model resolution. However, mesoscale resolution globally is not possible due to computational constraints. One of the solutions to this dilemma is variable-grid modeling where fine resolution is used over an area of interest and a coarser grid is used outside of this region.

[6] Various modeling approaches on variable grids have been widely applied to regional meteorological models (e.g., *Phillips* [1979]; the review by *Koch and McQueen* [1987]; *Pielke et al.* [1992]) and global numerical weather prediction models [*Courtier and Geleyn*, 1988; *Yessad and Benard*, 1996; *Coté et al.*, 1993] over the last decade. Nested grid CTMs have been used recently in regional air quality studies [*Byun and Ching*, 1999]. *Jacobson* [2001] developed a gas, aerosol, transport, radiation, general circulation and mesoscale meteorological model with a nesting feature to study urban to global scale atmospheric processes. Nested grid schemes have been known to have severe computational noise because of the abrupt change of grid resolution at the boundary. Therefore long-term computation is not possible without updating initial and boundary conditions periodically. These periodic updates of initial and lateral boundary conditions result in a predominantly one-way interaction between the coarse- and fine-resolution areas. An adaptive-grid meteorological and chemical transport model capable of horizontal resolution ranging from hundreds of kilometers to 1 km has been developed by *Bacon et al.* [2000] and tested by *Boybeyi et al.* [2001]. A global CTM on a stretched grid was first used by *Allen et al.* [2000] and has been used for tracer transport calculations. A stretched grid has an advantage over a nested grid because no lateral boundary conditions are needed. A stretched-grid model uses fine resolution over an area of interest, such as central and eastern North America, and outside of this region the grid size expands by a constant stretching factor, reaching a maximum grid size on the opposite side of the globe from the fine resolution region. Furthermore, the stretched grid model provides self-consistent interactions between global and regional scales of motions [*Fox-Rabinovitz*, 2000; *Fox-Rabinovitz et al.*, 2001, 2002]. We have developed a version of the University of Maryland Chemical Transport Model

(UMD-CTM) containing this stretched-grid feature, such that regional-to-global transport and chemistry can be more accurately represented.

[7] The global 3-D UMD-CTM (uniform and stretched frameworks [*Park et al.*, 2004]) was used to simulate the month of June 1985. In the stretched-grid simulation the fine horizontal resolution was focused over the central United States, where the PRESTORM field campaign was conducted. The Kansas/Oklahoma PRESTORM [*Cunning*, 1986] campaign was designed to study the organization, development, and evolution of mesoscale convective systems (MCSs) in the central United States, and utilized a wide variety of surface, satellite, and aircraft observing platforms. Chemical measurements during PRESTORM emphasized study of the redistribution of emissions by convection, and the scavenging mechanisms during convection [*Dickerson et al.*, 1987; *Pickering et al.*, 1988, 1989; *Luke*, 1990; *Luke et al.*, 1992]. The results provided by the global 3-D UMD-CTM were compared with these chemical measurements. The main objective was to examine the effects of deep convection and mesoscale weather systems on trace gas mixing ratios and on tropospheric ozone production over the central United States. We examine the transport and chemistry of the resulting convective plumes which exit the east coast of the United States. We also estimate the fluxes of CO, NO_x, NO_y, and O_3 at the east and west coasts of North America and emphasize the export of these gases in the free troposphere where due to longer chemical lifetimes and greater wind speeds the likelihood of long-range transport is enhanced over that for export in the boundary layer. We also compare the boundary layer export of these species with previous calculations.

[8] In section 2 we describe numerical experiments performed using the UMD-CTM. In section 3 we compare the model results for mesoscale features with flight measurements. The effects of deep convection and mesoscale weather systems on trace gas mixing ratios and on tropospheric ozone are discussed in section 4, and section 5, respectively. The export and import of O_3 and its precursors from and to the United States are analyzed in section 6. Conclusions of this study are formulated in section 7.

2. Model Experiment Description

[9] The UMD-CTM was described in detail in *Park et al.* [2004]. Here we describe it briefly in terms of the experimental design. The UMD-CTM is driven by the Goddard Earth Observing System Data Assimilation System (GEOS DAS) from the NASA Goddard Global Modeling and Assimilation Office (GMAO). The routinely available assimilated meteorology for 1985 is from the GEOS-1 DAS [*Schubert et al.*, 1993]. A UMD-CTM simulation with GEOS-1 DAS meteorology on a 4° × 5° uniform grid was performed for the entire year of 1985, and extensive evaluation of the results was conducted through comparisons with a variety of measurements [*Park et al.*, 2004].

[10] We performed three global simulations with the UMD-CTM for the PRESTORM experimental period over the month of June 1985. Each simulation uses different GEOS assimilated meteorology: GEOS-1 on a 2° × 2.5° uniform grid, GEOS-3 on a 2° × 2.5° uniform grid and the GEOS-3 stretched grid DAS (SG-DAS). By performing these multiple simulations for the same period with different meteorology we were able to distinguish the individual contributions to improvement in chemical species simulations from both changes in data assimilation system (GEOS-1 versus GEOS-3) and the use of a different grid scheme (uniform grid versus stretched grid).

[11] The stretched-grid version of the UMD-CTM is driven by the assimilated meteorology from the GEOS-3 Stretched Grid Data Assimilation System (SG-DAS) [*Fox-Rabinovitz*, 2000; *Fox-Rabinovitz et al.*, 2002] that contains the Stretched Grid-GCM (SG-GCM) [*Fox-Rabinovitz et al.*, 1997, 2001]. The GEOS-3 stretched-grid data assimilation was performed by using a horizontal domain size of 360 × 181 grid cells and 48 sigma layers extending from the surface to 0.01 hPa. The high resolution region in the SG-DAS was chosen to be over the central United States and extended from 112.05° to 86.55°W and 26.70° to 44.20°N with grid size of 0.5° × 0.5°. The grid is stretched outside of this region to a maximum grid size of 2.0° × 1.7° on the opposite side of the world. In the SG-DAS the dynamical calculations are performed on the stretched grid, but the model's physical routines are computed on a 1° × 1° uniform grid and results are interpolated to the stretched grid. Both the stretched and uniform GEOS-3 assimilations were initialized using the output from the GEOS-1 DAS approximately one month prior to June 1985. However, the GEOS-3 DAS physics and dynamics were different from the GEOS-1 DAS. Therefore noticable differences in calculated meteorology from the GEOS-1 exist due to the different model. In the GEOS-3 SG-DAS output differences are due to both the change of the model and the finer grid and are discussed in later sections.

[12] In order to reduce memory requirements for the chemistry simulations, we mapped the GEOS-3 SG-DAS meteorology onto a coarser model grid as follows. First, a new stretched grid was generated with a larger stretching factor, keeping the same fine resolution (0.5° × 0.5°) within the region of interest. The size of the new stretched grid became 256 × 129 grid cells, with maximum grid size of 3.8° × 3.7°. The SG-DAS meteorology was placed onto the new stretched grid using a horizontal mapping algorithm (S.-J. Lin, personal communication, 2001). Second, we decreased the number of layers by combining them in the stratosphere because the UMD-CTM focuses mainly on tropospheric chemistry. In addition, transport calculations in the stretched-grid version of the CTM on sigma surfaces tend to be noisy in the stratosphere. In order to reduce the magnitude of this problem, we used a hybrid sigma-pressure coordinate system. A total of 25 vertical layers were selected extending from the surface to 10 hPa with 17 sigma layers below 242 hPa from the SG-DAS and 8 constant pressure layers above 242 hPa to be approximately at the same pressures as the uppermost 8 layers of the GEOS-1 DAS. The same regridding was applied to the GEOS-3 DAS on the 2° × 2.5° uniform grid. Figure 1 shows vertical coordinates used in the GEOS-3 DAS (uniform- and stretched-grid) and the versions of the UMD-CTM.

[13] Both the uniform and the stretched grid UMD-CTM are initialized using the results provided by the 4° × 5° global uniform-grid UMD-CTM simulation of *Park et al.* [2004] at 00 UTC 01 June 1985. The same chemical scheme, emission inventories, and input data: total column

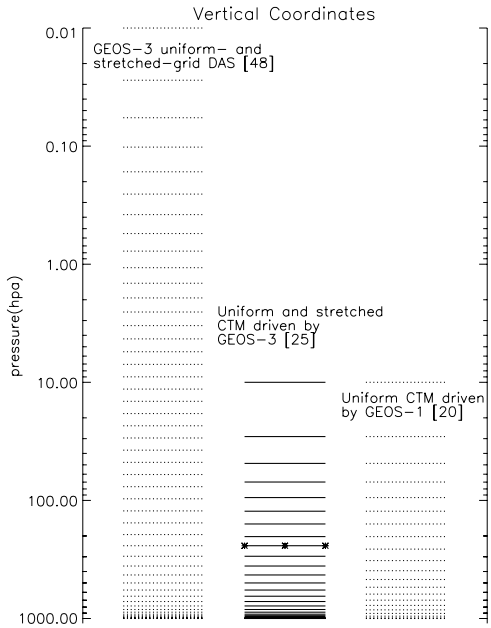

Figure 1. Vertical grids used in the GEOS-3 DAS (uniform- and stretched-grid) and in the UMD-CTM simulations.

ozone, the surface type data, and sulfate mixing ratios for heterogeneous chemistry were used in all three simulations. The numerical time step for each process in the model (e.g., advection, convection, and chemistry) was 15 minutes.

3. Model Evaluation on the Mesoscale

[14] Figure 2 demonstrates the ability of the stretched-grid model to represent the urban plumes from individual major cities. The plots of CO and NO_x show plumes from Chicago (41.5°N, 87.4°W), Denver (39.4°N, 105.0°W) , St. Louis (38.4°N, 90.1°W), Kansas City (39.0°N, 99.4°W), Dallas (32.5°N, 96.5°W), Houston (29.5°N, 96.2°W), New Orleans (29.6°N, 90.1°W) , Little Rock (34.4°N, 92.2°W), among others. These plumes are averaged out and not readily evident in the 2° × 2.5° output also shown in Figure 2. Grids of this size are typical of global models. When NO_x is artificially diluted in this manner, photochemical production of ozone is likely overestimated [*Chatfield and Delany*, 1990]. We have computed net ozone production by comparing the mass of ozone in a specified domain before and after each time the chemistry step is performed in the model. Calculations for the domain of Figure 2 were performed for a 12-hour period in the stretched-grid and uniform-grid versions of the model and are summarized in Table 1. The ozone production was estimated for the lowest 1, 6, and 9 model layers. Net ozone production on the 2° × 2.5° uniform grid is ∼15% larger than that in the stretched grid on 13 June, using the same strength of precursor emissions. This result reflects more efficient ozone production associated with the artificially diluted NO mixing ratios in the larger grid cells. Ozone production on the stretched grid is likely more accurate. The size of fine grid boxes (∼50 km) in the stretched-grid model simulation is approximately equivalent to the horizontal dimension of many of the urban areas shown in Figure 2, allowing these plumes to be depicted. However, precursor emissions in those areas are not uniform, as represented by the model, because a substantial fraction of those emissions are due to point sources. Therefore even higher horizontal resolution is needed to more accurately represent urban plumes.

[15] We will demonstrate the ability of the stretched-grid version of the model to represent mesoscale phenomena such as redistribution of trace gases by convection and the strong gradients of trace gases across a cold front. Aircraft observations of trace gases were conducted over Kansas and Oklahoma during June 1985 and have been reported by *Dickerson et al.* [1987], *Pickering et al.* [1988, 1989], and *Luke et al.* [1992]. In addition to tropospheric profiling, these measurements were often conducted in the upper tropospheric outflow from deep convective storms. Convection is one of the primary mechanisms for venting pollutants from the boundary layer and allowing them to reach altitudes at which they can be rapidly transported for long distances. We use these measurements to evaluate the uniform and stretched-grid models.

3.1. Model Convective Clouds

[16] The GEOS-DAS deep convection was first evaluated using synoptic weather analyses and infrared satellite

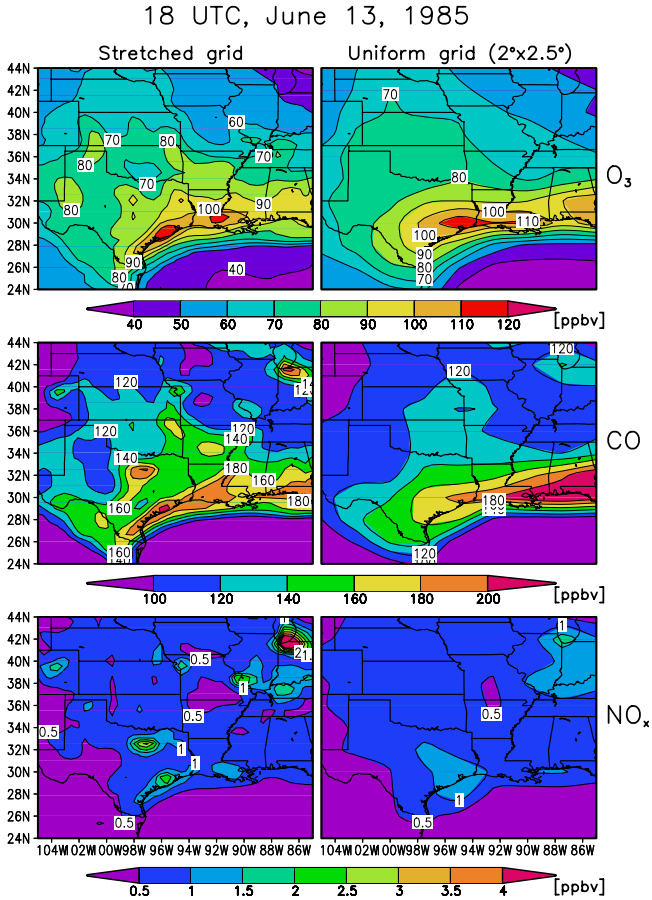

Figure 2. Simulated mixing ratios of (top) O_3, (middle) CO, and (bottom) NO_x averaged over the boundary layer for 18 UTC, 13 June 1985, in which numerous urban pollution plumes are represented in GEOS-3 stretched-grid and uniform-grid output.

Table 1. Net O_3 Production ($P(O_3)$) Between 1200 and 2400 UTC 13 June 1985 (10^8 moles/12 hrs)[a]

	$P(O_3)$ Lowest layer	$P(O_3)$ Lowest 6 layers	$P(O_3)$ Lowest 9 layers
Uniform grid (GEOS-3 2° × 2.5°)	2.7	52	74
Stretched grid (GEOS-3 SG)	2.3	45	63

[a]Summed over the domain shown in Figure 2.

images [*Meitin and Cunning*, 1985] as well as the International Satellite Cloud Climatology Project (ISCCP) cloud data for the month of June 1985. In these comparisons, we mainly focused on the convective activity over the PRESTORM region. Figure 3 shows three sets of GEOS-DAS deep convective cloud mass fluxes and ISCCP deep convective cloud observations averaged over the analyses for 1800 UT for each day during June, 1985. ISCCP deep convective cloud is defined to be cloud with cloud top pressures of <440 hPa and optical depth (τ) of >22.63 [*Rossow et al.*, 1996]. The ISCCP cloud data have been compared with other cloud observations [*Rossow et al.*, 1993]. For deep convective clouds over midlatitude continental regions no significant biases were noted. The ISCCP daytime deep convective cloud fraction is available in each 2.5° latitude by 2.5° longitude ISCCP grid cell. The cloud fractions were calculated by dividing the total number of pixels in each cell with deep convective clouds by the total number of pixels. Comparisons between GEOS-1 cloud mass fluxes and ISCCP deep convective cloud fractions were previously performed globally for the 1990–1992 period [*Allen et al.*, 1997].

[17] The ISCCP deep convection maximizes along and north of the northern border of the PRESTORM region, stretching eastward into Missouri and Illinois. The GEOS-1 cloud mass flux maximizes in the northeastern part of the PRESTORM region and outside the northeast corner of the region. However, the GEOS-1 intense convection is much more widespread throughout the central U.S. than is suggested by the ISCCP data. For example, the ISCCP data show a considerable north-south gradient of deep convective cloud amount between Missouri/Illinois and the Gulf of Mexico, while the GEOS-1 data show a much weaker gradient. The region of most intense convection in the 2° × 2.5° GEOS-3 assimilation is considerably smaller than with GEOS-1. In fact, averaged over the PRESTORM region, the GEOS-3 cloud mass fluxes are approximately 60% of those from GEOS-1. The region of intense convection becomes even smaller and more realistic with the GEOS-3 SG assimilation. However, in both the uniform- and stretched-grid GEOS-3 data the convection maximizes somewhat farther south than was evident in the GEOS-1 and ISCCP data. It is interesting to note that the SG-DAS produces the most realistic convection even though the convective parameterization was implemented on an intermediate 1° × 1° uniform grid. Apparently, the improvement in the dynamical fields from the SG-DAS has a positive effect on the subgrid convection.

[18] Figure 4 shows meteorological data from the GEOS-3 and SG DAS as well as CO data from the uniform-grid UMD-CTM and the stretched-grid UMD-CTM for a case of deep convection ahead of a cold front across western Oklahoma and the Texas Panhandle. The horizontal wind data at 950 hPa are shown from both the 2° × 2.5° GEOS-3 and SG-DAS (note shift from SW to NW across the cold front). The cold frontal position is more sharply defined in the finer-resolution SG-DAS data. Higher values of CO mixing ratio were pumped up to 240 hPa in the convection ahead of the front. Descending air behind the front leads to much lower CO mixing ratios. The horizontal differences of CO across the front are ~15 ppbv for the uniform grid UMD-CTM simulations and ~25 ppbv for the stretched-grid UMD-CTM simulations. Although the CO mixing ratios in the model are smaller than observed (see *Park et al.* [2004] for possible reasons), the difference from the stretched-grid version very closely matches the cross-frontal difference found in the aircraft observations at 10 km (~25 ppbv based on averages of 119 ppbv ahead of the front and 94 ppbv behind the front).

3.2. Model Comparison With Aircraft Composite Observations

[19] The sensitivity of model results to the driving meteorological data sets is analyzed by comparing model

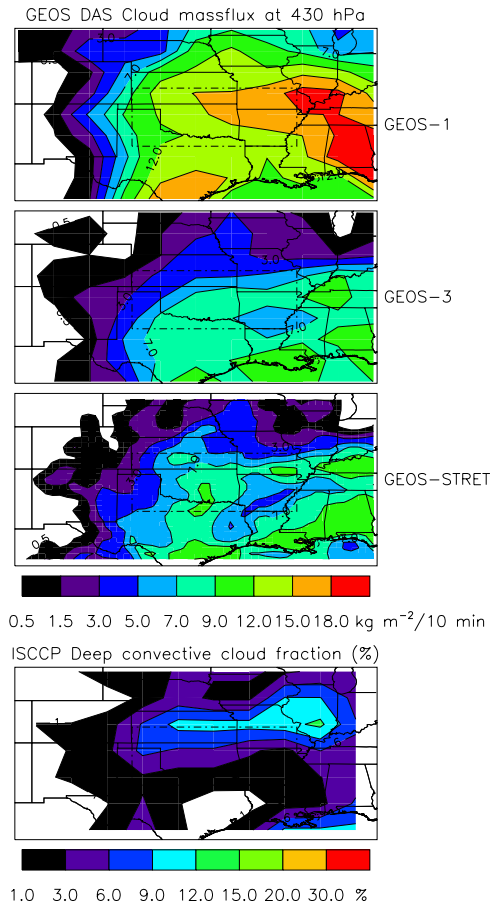

Figure 3. Comparisons of three sets of GEOS-DAS convective mass fluxes with ISCCP deep cloud fraction. GEOS-DAS convective mass fluxes at 430 hPa are averaged for 18 UTC over the month of June 1985, and ISCCP deep convective cloud fraction is averaged over daytime hours of the same month. Dash-dot line encloses the PRESTORM flight region.

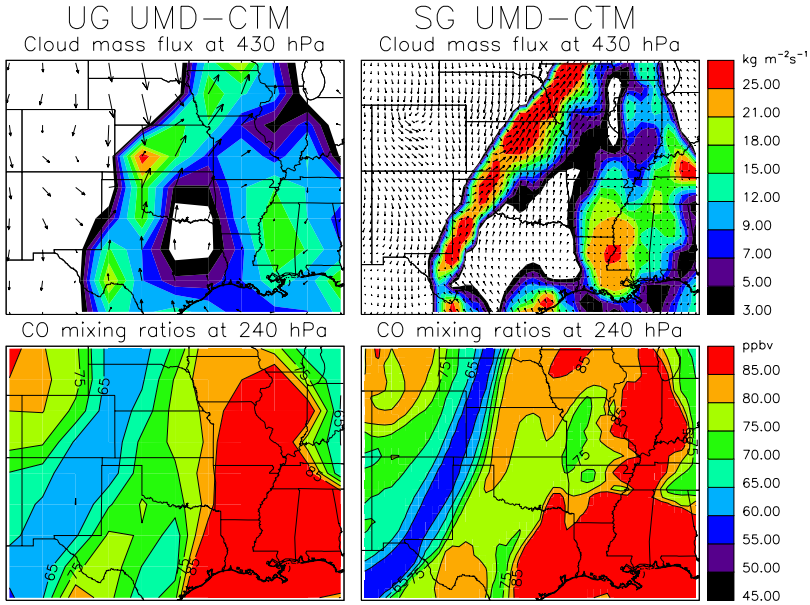

Figure 4. (top) Wind vectors at 950 hPa and upward cloud mass flux (kg m^{-2} s^{-1}) at 430 hPa, 1800 UTC, 26 June 1985 from (left) GEOS-3 DAS and (right) SG-DAS; (bottom) CO mixing ratios for same time at 240 hPa from (left) uniform-grid UMD-CTM (2° × 2.5°) with GEOS-3 DAS and from (right) stretched-grid UMD-CTM.

results with trace gas composite profiles [*Luke et al.*, 1992] for the synoptic flow regimes established for the PRESTORM region by *Ryan et al.* [1992]. The observed data were composited into polar (P) and maritime tropical (mT) regimes based on observed flow characteristics on the flight days. Within these general flow patterns, subcategories representing modified conditions (P(mod), mT(mod)) were identified following the meteorological analysis by *Ryan et al.* [1992]. The composites include all measurements from the 18 flights over the PRESTORM period. Results provided by the UMD-CTM simulations with three sets of GEOS-DAS data were extracted from the output data sets for the flight days and composited in the same manner. Since the mT and mT(mod) regimes are associated with deep convection and the flight measurements were generally made close to the convective events in time and location [*Luke*, 1990], only output on the measurement days from grid cells in the PRESTORM region where the cloud mass fluxes at 427 hPa were larger than 0.02 kg m^{-2} s^{-1} were selected. These selected model values then were averaged over the PRESTORM region and all of the flights in the synoptic regime. Data from all grid cells in the PRESTORM region were used in constructing the composite model profiles covering the days with P and P(mod) conditions.

3.2.1. CO

[20] Because the main source of CO emissions is from the surface, rapid increases in CO in the upper troposphere reflect vertical transport of high CO from the surface by upstream or local convection. Therefore we consider CO as a good tracer for convective transport, at least on a local scale. Figure 5 shows comparisons between the observed CO and the calculated CO according to the flow characteristics: combined polar and modified polar flow, modified maritime tropical flow, and maritime tropical flow. In the polar flow regime, no convection was observed and the flow was characterized as convectively stable, confining the surface emission of pollutants to the shallow mixed layer [*Luke et al.*, 1992]. Therefore the largest boundary layer values are observed in this regime, and the CO mixing ratios decrease rapidly with altitude with the observations showing no significant vertical mixing. However, the three sets of model output show increasing CO between 5 and 10 km, indicative of excessive upstream convection or convection occurring in the model on days on which none was observed.

[21] In the modified maritime tropical flow, a dry capping layer in the lower troposphere led to deep, locally focused convective activity [*Carlson et al.*, 1983; *Ryan et al.*, 1992]. CO mixing ratios decrease sharply in the lower troposphere, and in the lower to middle troposphere they are even smaller than concentrations at corresponding altitudes observed in polar flow. However, in the upper troposphere, CO has the largest values among the three regimes, reflecting the efficient convective transport of polluted boundary layer air. The calculated CO profiles show increases above 5 km and also reach the largest values of the three regimes in the upper troposphere. In the maritime tropical flow, conditional instability was observed with a deep mixed layer, and convection was less deep than in the modified maritime tropical regime [*McNamara*, 1988; *Ryan*, 1990; *Ryan et al.*, 1992]. Therefore the profile of CO observations shows a relatively uniform distribution up to 4 km reflecting the deep mixed layer, which the model meteorology did not simulate properly. The CO in the middle and upper troposphere is less than that found in the modified maritime tropical flow, suggesting a lesser frequency of large vertical development of the convection. Also the calculated CO is less than the calculated CO in modified maritime tropical flow in the middle and upper troposphere.

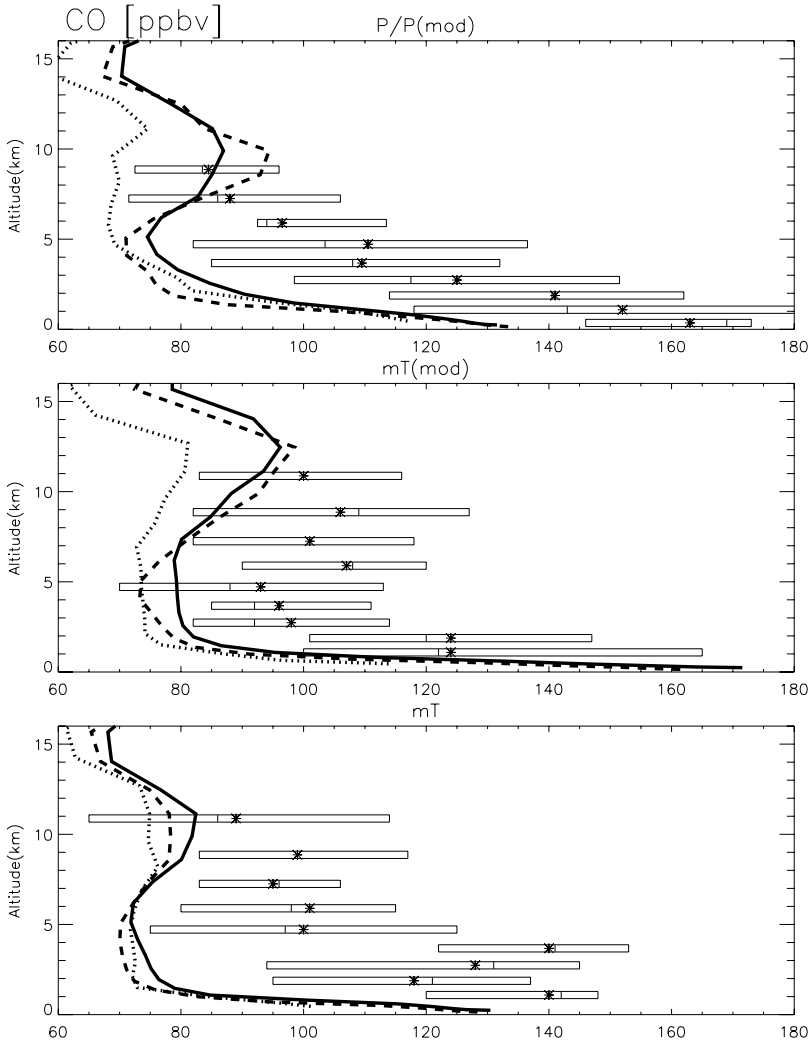

Figure 5. Vertical profiles of CO. Box represents 90% of measurements and vertical bar and asterisk are median and mean of measurements, respectively. The solid, dotted, and dashed lines are the mean of the model results provided by UMD-CTM simulations with SG-DAS, GEOS-1 DAS, and GEOS-3 DAS meteorology, respectively.

[22] In all three regimes at most altitudes the stretched-grid version of the model produced CO mixing ratios slightly closer to the observations than did the uniform-grid versions. We note that these improvements in CO comparisons are partly due to the use of stretched grid and more significantly due to changes in assimilated meteorology from GEOS-1 to GEOS-3. Also, in all three regimes the GEOS-1 profile shows the greatest deviation from the observations in the upper troposphere. The overestimate of deep convection in the GEOS-1 assimilation (Figure 3) vents CO too frequently from the boundary layer and does not allow the build-up of CO as seen in the other models (note that the GEOS-1 boundary layer values of CO are the lowest of the three simulations). Most of the CO that is vented is advected downstream of the grid cells where the deep convection is located.

[23] A significant underestimation of CO in our model calculations over the central U. S. compared with the observations is noted. The three sets of simulated CO underestimated the abundance of CO by 20–40 ppbv throughout the lower troposphere, and by lesser amounts above 6 km. The evaluation of calculated CO over the United States in our companion paper [*Park et al.*, 2004] suggests either a possible error in the source strength of CO over North America or too large a sink due to an overestimate of OH related to neglect of aerosols. Another possible reason could be that too frequent and widely occurring convection in the model provides less chance for large CO accumulation in the PBL that would be available for transport in the upper troposphere.

3.2.2. NO

[24] Figure 6 shows comparisons for NO. For all three regimes, profiles of NO resemble a C shape, reflecting the source from the lower and upper troposphere and the lack of sources in the middle troposphere. The model results here reflect both the convective transport of pollution from the boundary layer and the production of NO by lightning as parameterized through the cloud mass flux method of *Allen and Pickering* [2002]. Relatively lower NO mixing ratios in upper troposphere are seen in the polar flow category compared with the other regimes, revealing the minimal amount of convective activity both in the observation and

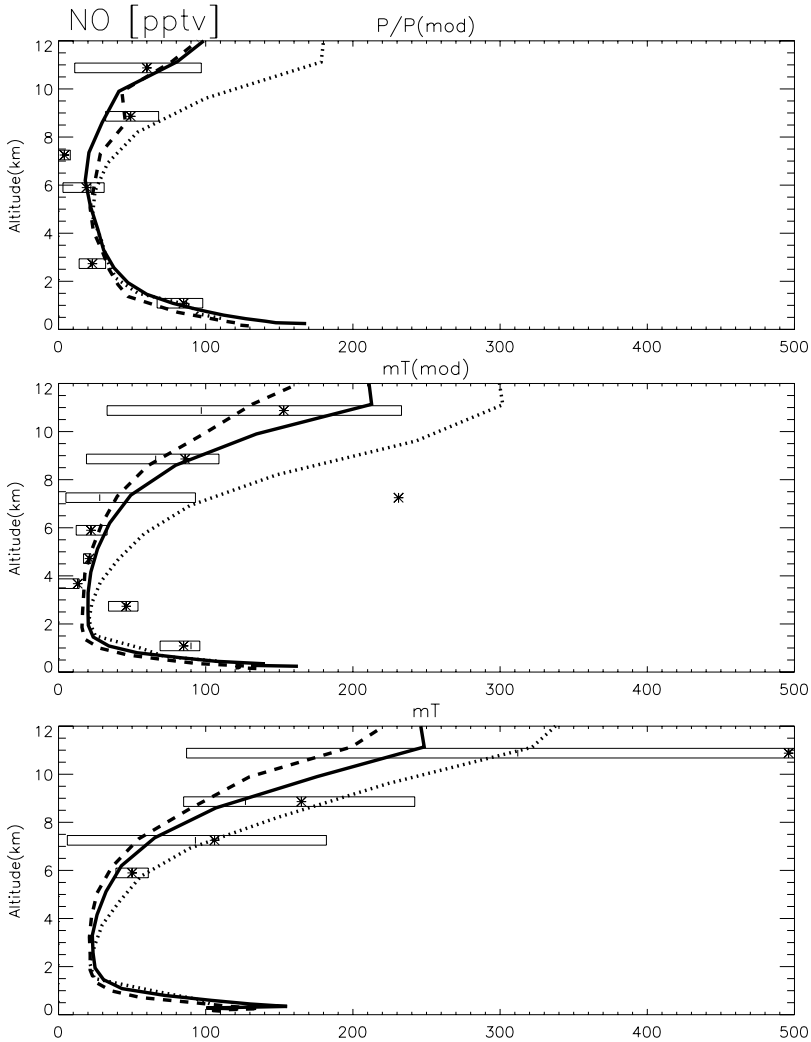

Figure 6. Same as Figure 5 but for NO.

the calculations. However, the GEOS-1 results overestimate the NO in the upper troposphere likely due to excessive convection, which leads to excessive lightning NO production in the model. For maritime tropical flow regimes, strongly elevated NO mixing ratios are shown in the upper troposphere, reflecting the considerable lightning activity and convective transport that corresponds with stronger convective activity than that in polar flow. The observations show that the NO mixing ratios in mT mode are larger than in mT(mod) indicating stronger lightning NO_x emissions in mT than in mT(mod). The calculated NO, however, does not differ significantly between the two modes. Overall, the calculated NO from simulations driven by the GEOS-3 DAS and GEOS-3 SG-DAS agree well with the observations. NO from the simulation driven by the GEOS-1 DAS tends to overestimate NO, particularly in the polar and mT(mod) regimes.

4. Sensitivity Studies for Deep Convection

[25] A sensitivity study examining the impact of deep convection was conducted by turning off the parameterized convective transport in the UMD-CTM during a convective episode that consisted of storms from Iowa to Texas on 15 June 1985. This episode contains the mesoscale convective complex (MCC) sampled by *Dickerson et al.* [1987]. UMD-CTM simulations driven by both the stretched-grid DAS and uniform-grid GEOS-3 DAS were used in this case. Resulting CO fields were subtracted from the corresponding CO fields from the stretched-grid and uniform-grid model runs containing convective transport to determine the differences caused by convection.

[26] Figures 7 and 8 show the difference fields from the stretched-grid and uniform-grid models, respectively, for three times on this date. Positive values represent increases in CO mixing ratios due to the vertical transport of the PBL air by deep convection in the 15 June events. The simulated convection started at 18 UTC 14 June 1985 and peaked at 00 UTC 15 June 1985. The deep convection caused increases of CO exceeding 24 ppbv at 10.6 km in the regions downstream of some of the most intense cells in the stretched-grid run. Peak differences from the uniform-grid simulations are smaller than those from the stretched-grid runs. A large area influenced by the convection shows increases of CO exceeding 12 ppbv in both sets of output. This CO plume can be seen

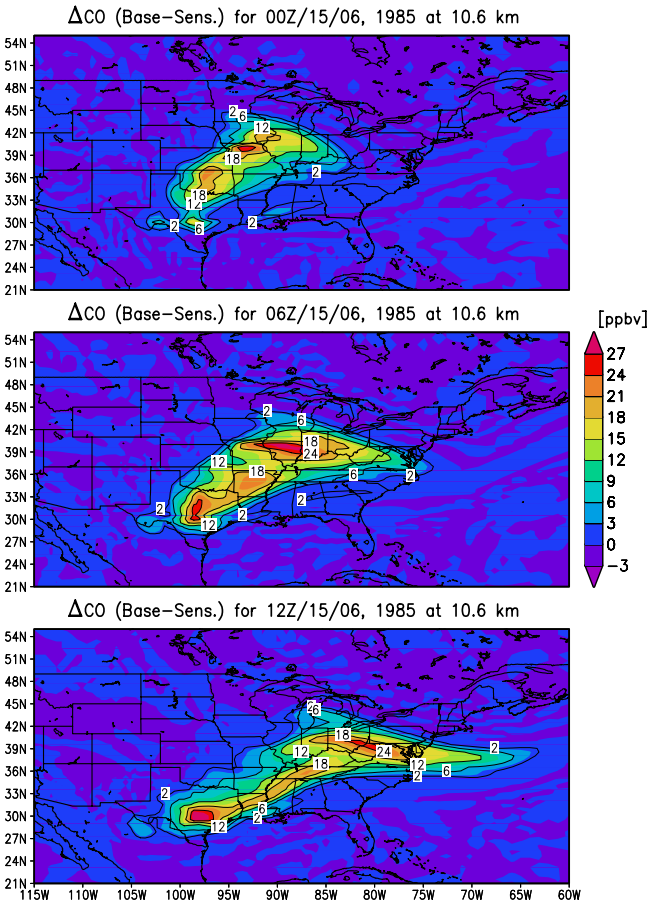

Figure 7. Difference (Δ CO) between CO fields from the stretched-grid UMD-CTM model simulations with convection (base) and without convection (sensitivity) at 10.6 km on 15 June 1985.

quickly exiting the east coast of the U.S. by 12 UTC. Increases in CO averaged over the stretched-grid model grid cells where the magnitude of the increase in CO is greater than 1 ppbv are 10.1 and 9.2 ppbv for 6 and 12 UTC, 15 June, respectively. The corresponding values for the uniform-grid simulation are 7.8 and 7.3 ppbv for these same times. Table 2 shows an increase in CO mass at 10.6 km due to parameterized deep convection on 15 June for both uniform and stretched grid model simulations, summed over the domain shown in Figures 7 and 8. The increase in CO in the stretched grid simulation is 30–60% larger than that of uniform grid simulation. For this particular event the stretched grid model simulation has lofted more CO from the boundary layer than the 2° × 2.5° uniform grid simulation. Measurements of CO recorded in background air unaffected by convection over Kansas and Oklahoma, as well as measurements taken in the convective outflow on 15 June are shown in Figure 9. The difference between these two sets of measurements is shown in the bottom panel of this figure. Differences of 20–30 ppbv were observed in the middle and upper troposphere in the convective outflow of an intense MCC. Therefore the model appears to be producing a convective impact in the upper troposphere of reasonable magnitude. The stretched-grid peak differences (24–27 ppbv) better correspond to the measured CO enhancements in the 15 June storm than do those from the uniform grid (15–24 ppbv).

5. Ozone Production Downstream of Deep Convection

[27] In this section, we examine photochemical ozone production downstream of deep convection over the PRESTORM region. As discussed previously, due to the boundary layer pollutants that are transported upward in the convection, as well as the additional NO_x injected from lightning, photochemical ozone production is enhanced downwind of deep convection in the middle and upper troposphere.

[28] We have computed the average ozone mixing ratio from the stretched-grid model at 9 km over 15 and 16 June 1985 (the period immediately following the convective episode described above) and over the period just prior to the convection (13–14 June). The difference, which ranges from near zero to over 25 ppbv, is shown in Figure 10, reflecting the enhancements due to ozone transport from the boundary layer and due to photochemical production in the convective outflow resulting from transport of precursors. Increases in ozone in the upper troposphere can also result from the intrusion of stratospheric ozone

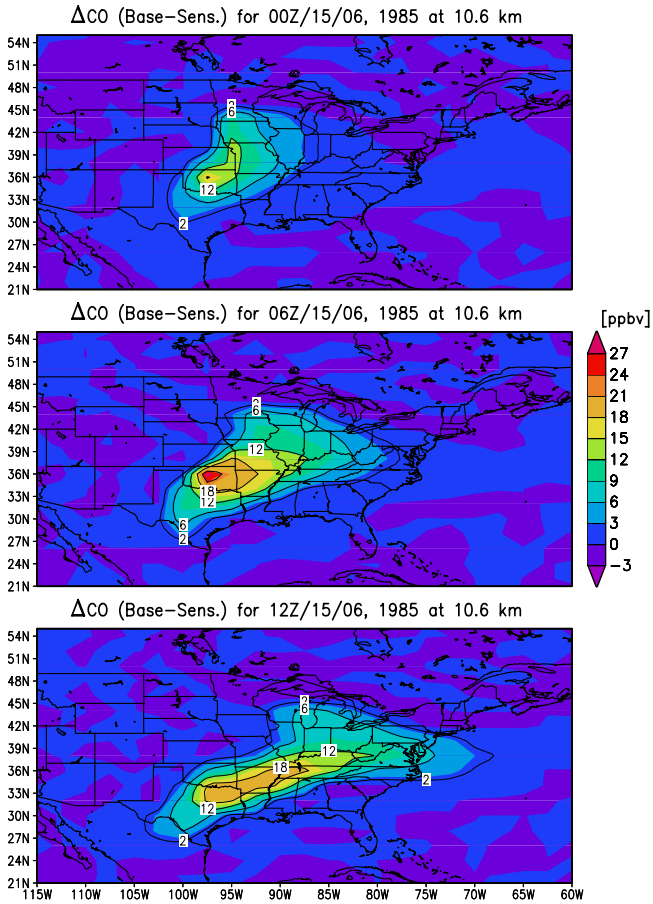

Figure 8. Difference (Δ CO) between CO fields from the uniform-grid UMD-CTM model simulations using GEOS-3 DAS meteorology with convection (base) and without convection (sensitivity) at 10.6 km on 15 June 1985.

Table 2. Increases in CO Mass (Gg CO) at 10.6 km Due to Parameterized Deep Convection on 15 June 1985[a]

Model	Time		
	00Z/15 June	06Z/15 June	12Z/15 June
Uniform grid (GEOS-3 2° × 2.5°)	4.1	8.2	9.6
Stretched grid	6.6	10.7	11.7

[a]Increases in CO mass due to convection are summed over the domain shown in Figures 7 and 8.

following frontal systems. Stratospheric influx, however, appears not to be a major factor for this case based on the CO distribution shown in Figure 9. Negative changes in CO would have been noted if stratospheric air had intruded. The maximum O_3 difference is located over Tennessee and Mississippi, which is downstream of intense convection that occurred over Oklahoma. Measurements of ozone and ozone precursors recorded in the convective outflow on 15 June were used by *Pickering et al.* [1990] in a one-dimensional (1-D) photochemical model to estimate downstream ozone production rates. Ozone production in the convective outflow at 8–9 km was estimated at ~15 ppbv for the first 24 hours after the storm. Therefore the UMD-CTM appears to be transporting reasonable quantities of ozone precursors to the upper troposphere and the model chemistry appears to be operating comparably at these altitudes.

[29] Twenty-four hour averaged O_3 over the downstream region (95°–80°W, 30°–40°N) is 73.4 ppbv before the convection and is 80.4 ppbv after the convection at 9 km, which is the altitude of maximum detrainment in this case. Therefore a 7 ppbv average increase in ozone is due to convective transport and photochemical production following the convection. Averaged over a large area downstream NO_x mixing ratios are ~40 pptv before the convection but after the convection they are well over 100 pptv (not shown). The maximum increase in ozone is ~25 ppbv (see Figure 10). The average increase (7 ppbv) and the peak increase (~25 ppbv) from 3-D global simulations are quantitatively in good agreement with the convective enhancements from *Park et al.* [2001] who showed ~10 ppbv increase in ozone at 9 km for convection in rural air and ~20 ppbv increase for convection over urban areas for the first 24-hour period following the 10–11 June Kansas/Oklahoma PRESTORM convection using a Single Column Chemical Transport Model (SCCTM). The maximum total radiative forcing due to these ozone increases from the SCCTM is 0.45 and 0.65 W/m^2 for the rural and urban cases, respectively, on 12 June 1985, assuming clear sky conditions. The single-column results demonstrate the importance of the perturbation in upper tropospheric ozone resulting from deep convection, and the 3-D UMD-CTM results shown here portray the spatial extent of this perturbation.

[30] We have computed the net ozone production following the 10–11 June PRESTORM event in the stretched-grid and uniform-grid versions of the model with and without the parameterized convection. For each model the difference in net ozone production was computed from the simulations with and without convection, and the results at 10.6 km are plotted in Figure 11. Convective enhancements of net O_3 production during the first day (11 June) following convection from both uniform-grid and stretched grid simulations are consistent in spatial distribution, although peak values from the stretched-grid simulation are larger than that of uniform-grid simulation reflecting the more concentrated convective plume of boundary layer air. The production rate becomes smaller as convective plumes are advected and diluted downwind. Note the much greater growth in size of the convective plume in the uniform-grid output. Table 3 shows the total net O_3 production due to 10–11 June convection summed over the domain shown in Figure 11 on 11–13 June. Total net O_3 production rates from both simulations are consistent on 11 June. However, the uniform-grid simulation shows more efficient ozone production than the stretched-grid simulation on 12–13 June because of the more rapid dilution of the convective outflow plume as shown in Figure 11. This result is consistent with the results for net O_3 production in urban plumes presented in

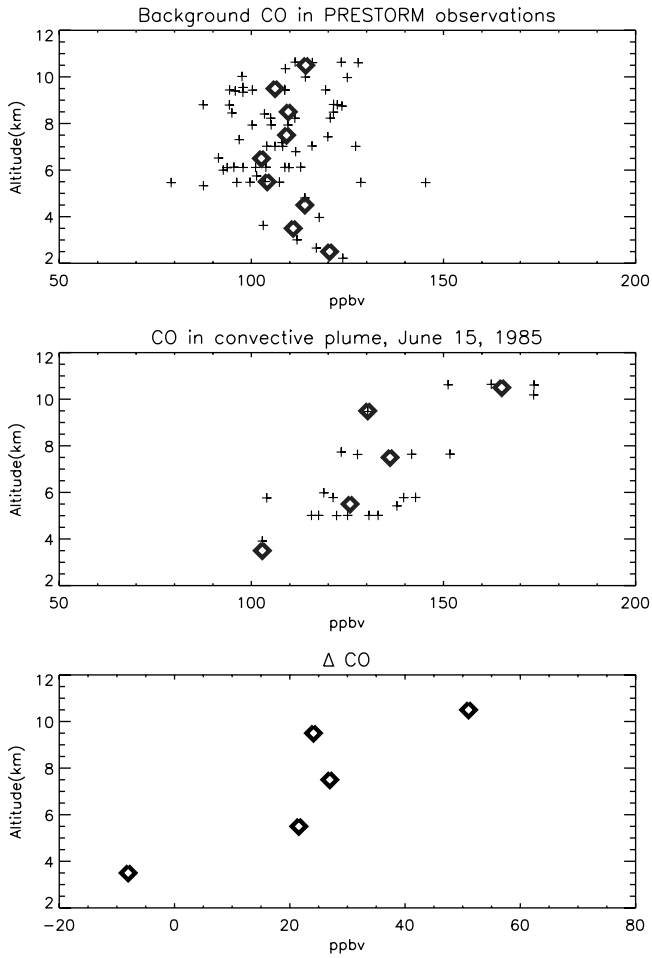

Figure 9. Composites of CO observations in PRESTORM campaign: (top) background CO measurements (no convection) over Kansas and Oklahoma; (middle) CO measurements in convective outflow on June 15, 1985 over eastern Oklahoma; (bottom) difference between cloud outflow and background data. Plus signs indicate individual 3-minute average measurements, while diamonds show 1-km layer averages.

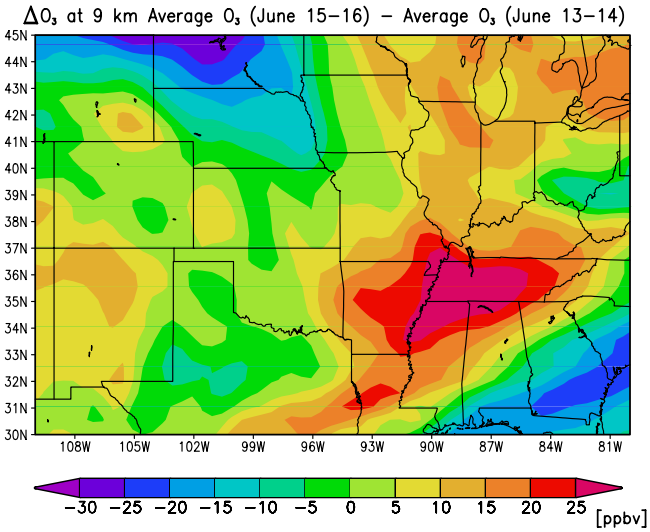

Figure 10. Average ozone at 9 km from stretched-grid UMD-CTM on 15–16 June (after convection) minus average ozone at 9 km on 13–14 June (before convection).

Section 3. Therefore we expect the net ozone production in the stretched-grid run to be more accurate.

6. North American Import and Export Fluxes

[31] We estimate the fluxes of CO, O_3, NO_x and NO_y imported to and exported from North America using the results from the stretched-grid UMD-CTM simulation for June 1985. The fluxes were computed using the CTM output and the GEOS-3 SG-DAS winds every 6 hours. Fluxes estimated from the GEOS-3 uniform-grid output differ by only a few percent. Figures 12 and 13 show daily fluxes of CO, O_3, NO_x, and NO_y from the stretched-grid model averaged over the month as functions of latitude and altitude, respectively. Export and import fluxes are estimated along the longitudes 65°W (North American east coast) and 130°W (west coast), respectively, in the region between 25 and 60°N. The fluxes are computed for the model levels below the approximate tropopause that varies with latitude. The fluxes shown in Figure 12 as a function of latitude have been normalized by the area of a column on the vertical plane. Therefore the fluxes are given as moles m^{-2}. Import fluxes are generally smaller than the export fluxes. The NO_x import fluxes are especially small, reflecting relatively low background concentrations due to the shorter lifetime compared with CO and ozone. The imports maximize around 45–50°N and at altitudes higher than 10 km, which are associated with the strong zonal wind in the jet stream. The model simulations do not show significant import fluxes of ozone and its precursors in the boundary layer. The maxima of export fluxes are shifted southward (35–40°N) relative to the import maxima, reflecting the location of North American emissions and the dominant transport pathways. The exports of NO_x and NO_y show a C-shaped profile (Figure 13), reflecting high NO_x concentrations in the boundary layer from the surface sources, as well as high concentrations at high altitude due to lightning NO_x production and convective transport of surface emissions.

[32] The model shows a significant enhancement in CO and ozone export fluxes compared to the import fluxes in the lower and middle troposphere. Our estimates of CO and ozone exports from North America between the surface and 7 km are 32 Gmol d^{-1} and 23 Gmol d^{-1}, respectively, compared with imports of 20 and 13 Gmol d^{-1} (see Table 4). Therefore our value for the net flux of ozone from North America in the lowest 7 km is 10 Gmol d^{-1} (23 minus 13 Gmol d^{-1}). This includes the direct boundary layer export, plus ozone that has been vertically transported from the boundary layer. In addition, it includes ozone produced photochemically in the free troposphere over North America. Therefore we estimate the contribution of North American anthropogenic and natural emissions of NO to ozone export in the lowest 7 km is 10 Gmol d^{-1}. We expect that during the month of June, the stratospheric contribution to tropospheric ozone is relatively small. However, we have chosen to compute the fluxes for the lowest 7 km to minimize any influence of stratospheric ozone.

[33] The export of ozone in the boundary layer below 2.5 km is 5.68 Gmol d^{-1}, while the import flux is 0.80 Gmol d^{-1} in this layer. Therefore North American emissions are causing a net export of 4.88 Gmol O_3 d^{-1} to

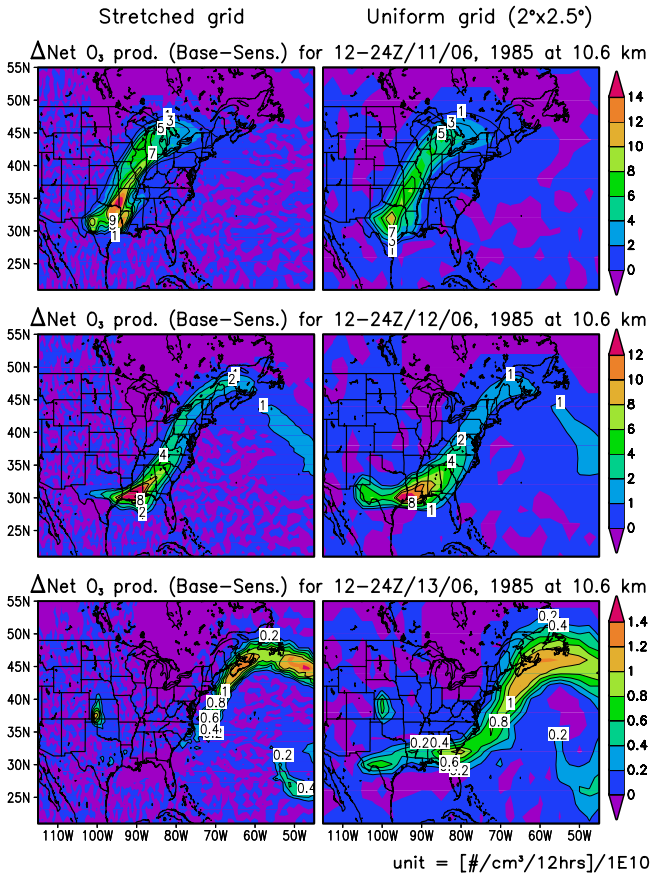

Figure 11. Difference (Δ net O_3 production) between net ozone production from UMD-CTM model simulations with convection (base) and without convection (sensitivity) at 10.6 km for 12–24 UTC on 11–13 June 1985. Results are shown for both the stretched-grid and uniform-grid versions of the model. Units are 10^{10} molecules cm^{-3} $(12\ hrs)^{-1}$.

Table 3. Net Ozone Production Downstream of Convection at 10.6 km on 11–13 June 1985 (10^8 moles/12 hrs)[a]

Model	Time 12–24Z/11 June	12–24Z/12 June	12–24Z/13 June
Uniform grid (GEOS3, 2 × 2.5)	2.3	2.2	0.69
Stretched grid	2.3	1.5	0.24

[a]Net ozone production summed over the domain shown in Figure 11.

the North Atlantic in this layer during June. Estimates of 4 Gmol d^{-1} and 6.5 Gmol d^{-1} for direct export of pollution-related ozone from the U. S. boundary layer have been published by *Jacob et al.* [1993] and *Liang et al.* [1998]. These estimates include vertical transport of ozone out of the boundary layer, which is not included in our boundary layer net export. However, these previous literature values do not account for ozone produced photochemically in the free troposphere due to ozone precursors vented from the boundary layer. Both of these components are included in our fluxes for the lowest 7 km.

[34] The NO_x and NO_y boundary layer exports are 0.01 Gmol d^{-1} and 0.11 Gmol d^{-1}, respectively. The literature estimates for boundary layer NO_x and NO_y export flux in previous studies [*Jacob et al.*, 1993; *Liang et al.*, 1998; *Horowitz et al.*, 1998] ranged from 0.07 to 0.12 Gmol d^{-1} and 0.30 to 0.35 Gmol d^{-1}, respectively. Again, these values include vertical transport from the boundary layer, while our lower estimates do not. Our net flux of NO_x in the lowest 7 km is 0.016 Gmol d^{-1}, which is still less than the literature estimates of boundary layer export. This result is likely due to the fact that the vertical export from the boundary layer in the previous estimates was computed over North America, whereas our estimate for the total troposphere is computed at the east coast, at which point most of the NO_x has been oxidized to other NO_y species. Therefore our 0–7 km net flux of 0.24 Gmol d^{-1} NO_y compares much better with the literature values. If the entire depth of the troposphere is considered, then our net flux is 0.38 Gmol d^{-1}, slightly exceeding the literature estimates most likely because it includes the full effect of lightning emissions. Our North American NO_x emission is 1.6 Gmol d^{-1}. Therefore our results show that only ~1% of the NO_x emitted is exported as NO_x and 15% of the NO_x emitted is exported as NO_y below 7 km. The total tropospheric NO_y flux is 24% of the emission value. The 1% NO_x export is smaller than others have found in previous work for the same reason expressed above concerning the absolute magnitude of the NO_x export. However, the 24% NO_y export is consistent with previous studies [*Kasibhatla et al.*, 1993; *Horowitz et al.*, 1998]. Large enhancements of the export flux of NO_x and NO_y over the import fluxes are noted at all altitudes up to 13 km (Figure 13). Less CO and ozone are exported than imported above 9 km, even though mixing ratios are generally larger at the east coast. This result is related to the stronger jet stream wind speeds over the Pacific compared with the Atlantic. Zonal wind speeds in the upper troposphere on the west coast are larger than those on the east by a greater amount than the CO and O_3 mixing ratios on the east coast are larger than those on the west. Therefore the import fluxes in the upper troposphere will be greater than the export fluxes for these species. Export of NO_x and NO_y below 13 km is greater than the import despite the wind speed difference, because of the substantial injection of NO by lightning in the upper troposphere over North America.

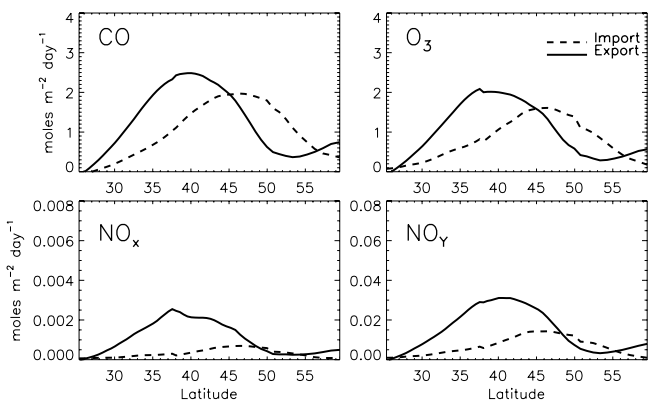

Figure 12. North American export and import fluxes of tropospheric CO, O_3, NO_x, and NO_y as a function of latitude. Export and import fluxes are defined at 65°W and 130°W, respectively.

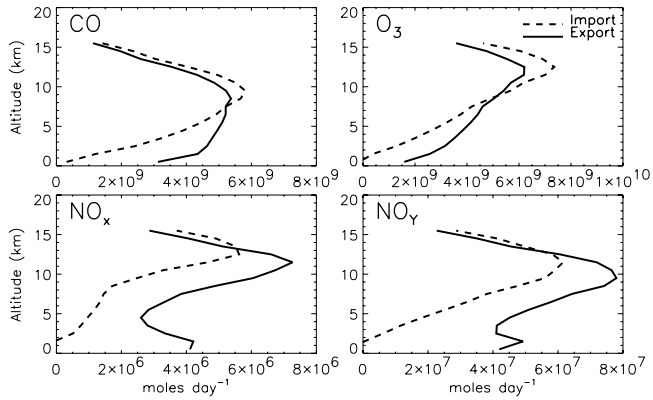

Figure 13. Profiles of North American export and import fluxes of CO, O_3, NO_x, and NO_y summed over the region between 25°N and 60°N, and at 65°W and 130°W, respectively.

7. Conclusions

[35] We have developed a new chemical transport modeling system that depicts urban plumes and mesoscale phenomena, such as the effect of fronts and convection on

Table 4. North American Import and Export Fluxes of Trace Gases (Gmol d^{-1})

Species	Free Troposphere (<7 km) Import	Free Troposphere (<7 km) Export	Boundary Layer (<2.5 km) Import	Boundary Layer (<2.5 km) Export
CO	20	32	2.6	9.8
O_3	13	23	0.80	5.68
NO_x	0.004	0.02	0.00	0.01
NO_y	0.09	0.33	0.00	0.11

trace gas mixing ratios, in an enhanced-resolution region of a global simulation. Comparisons with flight data from Kansas and Oklahoma have revealed that the model performs quite well in simulating the effects of mesoscale features. Enhancements of trace gases in the upper troposphere in convective outflow for specific events compare well with measurements. However, deep convection is too frequent and widespread over the central U. S., especially in the GEOS-1 data. Improvements are noted in the GEOS-3 data, and further improvement is seen in the GEOS-3 SG DAS.

[36] Comparisons with data composites for each flow regime show that the UMD-CTM is successful in simulating the shapes of the profiles after segregation by flow characteristics. However, the model (with each of the sets of meteorological input) tends to underestimate CO mixing ratios. The underestimation of CO over the central United States in the stretched-grid version of the model is similar to the underestimation of CO at North America stations and profiles shown in the uniform-grid model evaluations by *Park et al.* [2004]. The NO calculated with all three sets of GEOS-DAS meteorological fields is in reasonable agreement with observed profiles, but the NO calculated with GEOS-1 is the largest because of the overestimated convective activity (Figure 3) and associated lightning NO production.

[37] Comparisons between the 24-hour averaged ozone mixing ratios downstream before and after the 15 June 1985 convective event, as well as model sensitivity simulations showed that the differences in upper tropospheric CO and O_3 are in good agreement with the flight measurements. The stretched-grid output provided a better comparison with measured peak CO enhancements. Increases in trace gas mixing ratios in both model and measurements clearly demonstrate precursor transport to the upper troposphere and enhancement of photochemical O_3 production due to the deep convection. We have demonstrated that the artificial dilution of ozone precursors in the $2° \times 2.5°$ uniform-grid model leads to larger net ozone production rates in both boundary layer urban plumes and in upper tropospheric convective outflow plumes. Therefore we expect the stretched-grid output to be more accurate. Flight measurements over broad regions downwind of convection are needed to aid in verifying this result.

[38] Our stretched-grid model results have been used to estimate the import and export fluxes of trace gases at the coasts of North America. We compute the direct horizontal net export of ozone to be 4.88 Gmol d^{-1} in the boundary layer and 10 Gmol d^{-1} in the lowest 7 km. The latter includes ozone produced photochemically in the free troposphere over North America after precursors were vented from the boundary layer. This component of tropospheric ozone was not included in previously published export estimates.

[39] Many of the results from the stretched-grid UMD-CTM driven by assimilated meteorology are encouraging, showing reasonably accurate representation of mesoscale features and enhancement of trace gases in the upper troposphere due to convection. A benefit of the mesoscale resolution is more accurate photochemical ozone production in urban plumes and in convective outflow. The results provided from the PRESTORM simulations will be used in the future for estimating the effect of deep convection on changes in the global chemical budget and on climate using off-line radiative forcing calculations as an initial step toward a fully coupled GCM with chemistry.

[40] **Acknowledgments.** This research was supported under a NASA EOS Interdisciplinary Science Investigation (NASA grants NAG5-3678 and NAG5-9672).

References

Allen, D. J., and K. E. Pickering (2002), Evaluation of lightning flash rate parameterizations for use in a global chemical-transport model, *J. Geophys. Res.*, *107*(D23), 4711, doi:10.1029/2002JD002066.

Allen, D. J., K. E. Pickering, and A. Molod (1997), An evaluation of deep convective mixing in the Goddard Chemical Transport Model using International Satellite Cloud Climatology Project cloud parameters, *J. Geophys. Res.*, *102*, 25,467–25,476.

Allen, D., K. Pickering, G. Stenchikov, A. Thompson, and Y. Kondo (2000), A three-dimensional total odd nitrogen (NOy) simulation during SONEX using a stretched-grid chemical transport model, *J. Geophys. Res.*, *105*, 3851–3876.

Bacon, D. P., et al. (2000), A dynamically adapting weather and dispersion model: The Operational Multiscale Environment Model with Grid Adaptivity (OMEGA), *Mon. Weather Rev.*, *128*(7), 2044–2076.

Barth, M., A. Stuart, and W. Skamarock (2001), Numerical simulations of the July 10, 1996, Stratospheric-Tropospheric Experiment: Radiation, Aerosols, and Ozone (STERAO)-deep convection experiment storm: Redistribution of soluble tracers, *J. Geophys. Res.*, *106*, 12,381–12,400.

Berntsen, T. K., S. Karlsdottir, and D. A. Jaffe (1999), Influence of Asian emissions on the composition of air reaching the North Western United States, *Geophys. Res. Lett.*, *26*(14), 2171–2174.

Bey, I., D. J. Jacob, R. M. Yantosca, J. A. Logan, B. Field, A. M. Fiore, Q. Li, H. Liu, L. J. Mickley, and M. Schultz (2001), Global modeling of tropospheric chemistry with assimilated meteorology: Model description and evaluation, *J. Geophys. Res.*, *106*, 23,073–23,096.

Boybeyi, Z., N. N. Ahmad, D. P. Bacon, T. J. Dunn, M. S. Hall, P. C. S. Lee, R. A. Sarma, and T. R. Wait (2001), Evaluation of the operational multiscale environment model with grid adaptivity against the European tracer experiment, *J. Appl. Meteorol.*, *40*(9), 1541–1558.

Brasseur, G. P., D. A. Hauglustaine, and S. Walters (1996), Chemical compounds in the remote Pacific troposphere: Comparison between MLOPEX measurements and chemical transport model calculations, *J. Geophys. Res.*, *101*, 14,795–14,813.

Brasseur, G. P., D. A. Hauglustaine, S. Walters, P. J. Rasch, J.-F. Müller, C. Granier, and X. X. Tie (1998), MOZART, a global chemical transport model for ozone and related chemical tracers: 1. Model description, *J. Geophys. Res.*, *103*, 28,265–28,289.

Byun, D. W., and J. K. S. Ching (1999), Science algorithms of the EPA MODELS-3 Community multiscale air quality (CMAQ) modeling system, *EPA/600/R-99/030*, Environ. Protection Agency, Washington, D.C.

Carlson, T. N., S. G. Benjamin, G. S. Forbes, and Y. F. Li (1983), Elevated mixed layers in the regional severe storm environment: Conceptual model and case studies, *Mon. Weather Rev.*, *111*(7), 1453–1473.

Chatfield, R. B., and P. J. Crutzen (1984), Sulfur dioxide in remote oceanic air: Cloud transport of reactive precursors, *J. Geophys. Res.*, *89*, 7111–7132.

Chatfield, R. B., and A. C. Delany (1990), Convection links biomass burning to increased tropical ozone: However, models will tend to overpredict O_3, *J. Geophys. Res.*, *95*, 18,473–18,488.

Coté, J., M. Roch, A. Staniforth, and L. Fillion (1993), A variable-resolution semi-Lagrangian finite-element global model of the shallow-water equations, *Mon. Weather Rev.*, *121*(1), 231–243.

Courtier, P., and J.-F. Geleyn (1988), A global numerical weather prediction model with variable resolution: Application to the shallow-water equations, *Q. J. R. Meteorol. Soc.*, *114*(483), 1321–1346.

Crutzen, P. J., and L. T. Gidel (1983), A two-dimensional photochemical model of the atmosphere: 2. The tropospheric budgets of the anthropogenic chlorocarbons, CO, CH_4, CH_3Cl and the effect of various NO_x sources on tropospheric ozone, *J. Geophys. Res.*, *88*, 6641–6661.

Cunning, J. B. (1986), The Oklahoma-Kansas preliminary regional experiment for STORM-Central, *Bull. Am. Meteorol. Soc.*, *67*, 1478–1486.

DeCaria, A. J., K. E. Pickering, G. L. Stenchikov, J. R. Scala, J. L. Stith, J. E. Dye, B. A. Ridley, and P. Laroche (2000), A cloud-scale model study of lightning-generated NO_x in an individual thunderstorm during STERAO-A, *J. Geophys. Res.*, *105*, 11,601–11,616.

Dickerson, R. R., et al. (1987), Thunderstorms: An important mechanism in the transport of air pollutants, *Science*, *235*, 460–465.

Folkins, I., R. Chatfield, D. Baumgardner, and M. Proffitt (1997), Biomass burning and deep convection in southeastern Asia: Results from ASHOE/MAESA, *J. Geophys. Res.*, *102*, 13,291–13,299.

Fox-Rabinovitz, M. S. (2000), Regional climate simulation of anomalous U.S. summer events using a variable-resolution stretched-grid GCM, *J. Geophys. Res.*, *105*, 29,635–29,646.

Fox-Rabinovitz, M. S., G. L. Stenchikov, M. J. Suarez, and L. L. Takacs (1997), A finite-difference GCM dynamical core with a variable resolution stretched grid, *Mon. Weather Rev.*, *125*(11), 2943–2968.

Fox-Rabinovitz, M. S., L. L. Takacs, R. C. Govindaraju, and M. J. Suarez (2001), A variable-resolution stretched-grid general circulation model: Regional climate simulation, *Mon. Weather Rev.*, *129*(3), 453–469.

Fox-Rabinovitz, M. S., L. L. Takacs, and R. C. Govindaraju (2002), A variable-resolution stretched-grid general circulation model and data assimilation system with multiple areas of interest: Studying anomalous regional climate events of 1998, *J. Geophys. Res.*, *107*(D24), 4768, doi:10.1029/2002JD002177.

Gidel, L. T. (1983), Cumulus cloud transport of transient tracers, *J. Geophys. Res.*, *88*, 6587–6599.

Hauf, T., P. Schulte, R. Alheit, and H. Schlager (1995), Rapid vertical trace gas transport by an isolated midlatitude thunderstorm, *J. Geophy. Res.*, *100*, 22,957–22,970.

Horowitz, L. W., J. Liang, G. M. Gardner, and D. J. Jacob (1998), Export of reactive nitrogen from North America during summertime: Sensitivity to hydrocarbon chemistry, *J. Geophys. Res.*, *103*, 13,451–13,476.

Jacob, D. J., J. A. Logan, G. M. Gardner, R. M. Yevich, C. M. Spivakovsky, S. C. Wofsy, S. Sillman, and M. J. Prather (1993), Factors regulating ozone over the United States and its export to the global atmosphere, *J. Geophys. Res.*, *98*, 14,817–14,826.

Jacob, D. J., J. A. Logan, and P. P. Murti (1999), Effect of rising Asian emissions on surface ozone in the United States, *Geophys. Res. Lett.*, *26*(14), 2175–2178.

Jacobson, M. Z. (2001), GATOR-GCMM: A global- through urban-scale air pollution and weather forecast model: 1. Model design and treatment of subgrid soil, vegetation, roads, rooftops, water, sea ice, and snow, *J. Geophys. Res.*, *106*, 5385–5401.

Jaffe, D., et al. (1999), Transport of Asian air pollution to North America, *Geophys. Res. Lett.*, *26*(6), 711–714.

Jonquières, I., and A. Marenco (1998), Redistribution by deep convection and long-range transport of CO and CH_4 emissions from the Amazon basin, as observed by the airborne campaign TROPOZ II during the wet season, *J. Geophys. Res.*, *103*, 19,075–19,091.

Kasibhatla, P. S., H. Levy II, and W. J. Moxim (1993), Global NO_x, HNO_3, PAN, and NO_y distributions from fossil fuel combustion emissions: A model study, *J. Geophys. Res.*, *98*, 7165–7180.

Koch, S. E., and J. T. McQueen (1987), A survey of nested grid techniques and their potential for use within the MASS weather prediction model, *NASA Tech. Memo TM-87808*, 25 pp.

Lawrence, M. G., R. von Kuhlmann, M. Salzmann, and P. J. Rasch (2003), The balance of effects of deep convective mixing on tropospheric ozone, *Geophys. Res. Lett.*, *30*(18), 1940, doi:10.1029/2003GL017644.

Lelieveld, J., and P. J. Crutzen (1994), Role of deep cloud convection in the ozone budget of the troposphere, *Science*, *264*, 1759–1761.

Li, Q., et al. (2002), Transatlantic transport of pollution and its effects on surface ozone in Europe and North America, *J. Geophys. Res.*, *107*(D13), 4166, doi:10.1029/2001JD001422.

Liang, J., L. W. Horowitz, D. J. Jacob, Y. Wang, A. M. Fiore, J. A. Logan, G. M. Gardner, and J. W. Munger (1998), Seasonal budgets of reactive nitrogen species and ozone over the United States, and export fluxes to the global atmosphere, *J. Geophys. Res.*, *103*, 13,435–13,450.

Lu, R., C. Lin, R. Turco, and A. Arakawa (2000), Cumulus transport of chemical tracers: 1. Cloud-resolving model simulations, *J. Geophys. Res.*, *105*, 10,001–10,021.

Luke, W. T. (1990), Reactive nitrogen compounds in the troposphere: Observations, transport and photochemistry, Ph.D. thesis, Dept. of Chem., Univ. of Md., College Park.

Luke, W. T., R. R. Dickerson, W. F. Ryan, K. E. Pickering, and L. J. Nunnermacker (1992), Tropospheric chemistry over the lower Great Plains of the United States: 2. Trace gas profiles and distributions, *J. Geophys. Res.*, *97*, 20,647–20,670.

McNamara, D. P. (1988), Origin of ozone over central U.S., M.S. thesis, Dept. of Meteorol., Univ. of Md., College Park.

Meitin, J., Jr., and J. B. Cunning (1985), The Oklahoma-Kansas preliminary regional experiment for STORM-Central (O-K PRE-STORM), vol. I, Daily operations summary, *NOAA Tech. Memo., ERL ESG-20*.

Müller, J.-F., and G. Brasseur (1995), IMAGES: A three-dimensional chemical transport model of the global troposphere, *J. Geophys. Res.*, *100*, 16,445–16,490.

Park, R. J., G. L. Stenchikov, K. E. Pickering, R. R. Dickerson, D. J. Allen, and S. Kondragunta (2001), Regional air pollution and its radiative forcing: Studies with a single column chemical and radiation transport model, *J. Geophys. Res.*, *106*, 28,751–28.770.

Park, R. J., K. E. Pickering, D. J. Allen, G. L. Stenchikov, and M. Fox-Rabinovitz (2004), Global simulation of tropospheric ozone using the Univ. of Maryland Chemical Transport Model (UMD-CTM): 1. Model description and evaluation, *J. Geophys. Res*, D09301, doi:10.1029/2003JD004266.

Phillips, N. A. (1979), The nested grid model, *NOAA Tech. Rep., NWS22*, 80 pp.

Pickering, K. E., R. R. Dickerson, G. J. Huffman, J. F. Boatman, and A. Schanot (1988), Trace gas transport in the vicinity of frontal convective clouds, *J. Geophys. Res.*, *93*, 759–773.

Pickering, K. E., R. R. Dickerson, W. T. Luke, and L. J. Nunnermacker (1989), Clear-sky vertical profiles of trace gases as influenced by upstream convective activity, *J. Geophys. Res.*, *94*, 14,879–14,892.

Pickering, K. E., A. M. Thompson, R. R. Dickerson, W. T. Luke, D. P. McNamara, J. P. Greenberg, and P. R. Zimmerman (1990), Model calculations of tropospheric ozone production potential following observed convective events, *J. Geophys. Res.*, *95*, 14,049–14,062.

Pickering, K. E., J. R. Scala, A. M. Thompson, W.-K. Tao, and J. Simpson (1992a), A regional estimate of convective transport of CO from biomass burning, *Geophys. Res. Lett.*, *19*, 289–292.

Pickering, K. E., A. M. Thompson, J. R. Scala, W.-K. Tao, R. R. Dickerson, and J. Simpson (1992b), Free tropospheric ozone production following entrainment of urban plumes into deep convection, *J. Geophys. Res.*, *97*, 17,985–18,000.

Pickering, K. E., et al. (1996), Convective transport of biomass burning emissions over Brazil during TRACE A, *J. Geophys. Res.*, *101*, 23,993–24,012.

Pielke et al. (1992), A comprehensive meteorological modeling system-RAMS, *Meteorol. Atmos. Phys.*, *49*, 69–91.

Roelofs, G.-J., and J. Lelieveld (1995), Distribution and budget of O_3 in the troposphere calculated with a chemistry general circulation model, *J. Geophys. Res.*, *100*, 20,983–20,998.

Rossow, W. B., A. W. Walker, and L. C. Gardner (1993), Comparison of ISCCP and other cloud amounts, *J. Clim.*, *6*, 2394–2418.

Rossow, W. B., A. W. Walker, D. E. Beuschel, and M. D. Roiter (1996), International Satellite Cloud Climatology Project (ISCCP) Documentation of New Cloud Datasets, *WMO/TD 737*, 115 pp., World Meteorol. Org., Geneva.

Ryan, W. F. (1990), Synoptic scale variations in vertical ozone profiles over the lower Great Plains of the United States, M.S. thesis, Dept. Meteorol., Univ. of Md., College Park.

Ryan, W. F., R. R. Dickerson, G. J. Huffman, and W. T. Luke (1992), Tropospheric chemistry over the lower Great Plains of the United States: 1. Meteorology, *J. Geophys. Res.*, *97*, 17,963–17,984.

Schubert, S., J. Pfaendtner, and R. Rood (1993), An assimilated data set for earth science applications, *Bull. Am. Meteorol. Soc.*, *74*, 2331–2342.

Wang, C., and R. G. Prinn (2000), On the roles of deep convective clouds in tropospheric chemistry, *J. Geophys. Res.*, *105*, 22,269–22,297.

Wang, C., P. J. Crutzen, and V. Ramanathan (1995), The role of a deep convective storm over the tropical Pacific Ocean in the redistribution of atmospheric chemical species, *J. Geophys. Res.*, *100*, 11,509–11,516.

Wang, Y., D. J. Jacob, and J. A. Logan (1998), Global simulation of troposphric O_3-NO_x-hydrocarbon chemistry: 1. Model formulation, *J. Geophys. Res.*, *103*, 10,713–10,725.

Wang, Y., S. C. Liu, H. Yu, and S. T. Sandholm (2000), Influence of convection and biomass burning outflow on tropospheric chemistry over the tropical Pacific, *J. Geophys. Res.*, *105*, 9321–9333.

Yessad, K., and P. Benard (1996), Introduction of a local maping factor in the spectral part of the Meteo-France global variable mesh numerical forecast model, *Q. J. R. Meteorol. Soc.*, *122*(535), 1701–1719.

D. J. Allen and K. E. Pickering, Department of Meteorology, University of Maryland, 3411 Computer and Space Science Building, College Park, MD 20742, USA. (pickerin@atmos.umd.edu)

M. S. Fox-Rabinovitz, Earth System Science Interdisciplinary Center, University of Maryland, 2207 Computer & Space Sciences Building, College Park, MD 20742, USA.

R. J. Park, Division of Engineering and Applied Sciences, Department of Earth and Planetary Sciences, Harvard University, 29 Oxford Street, Cambridge, MA 02138, USA.

G. L. Stenchikov, Department of Environmental Sciences, Rutgers University, New Brunswick, NJ 08901, USA.